Sequential activation of necroptosis and apoptosis cooperates to mediate vascular and neural pathology in stroke

Masanori Gomi Naito[a], Daichao Xu[a], Palak Amin[a], Jinwoo Lee[a], Huibing Wang[a], Wanjin Li[a], Michelle Kelliher[b], Manolis Pasparakis[c], and Junying Yuan[a,1]

[a]Department of Cell Biology, Harvard Medical School, Boston, MA 02468; [b]Department of Molecular, Cell and Cancer Biology, University of Massachusetts Medical School, Worcester, MA; and [c]Institute for Genetics, University of Cologne, D-50674 Cologne, Germany

Contributed by Junying Yuan, December 18, 2019 (sent for review September 30, 2019; reviewed by Jun Chen and Robert M. Friedlander)

Apoptosis and necroptosis are two regulated cell death mechanisms; however, the interaction between these cell death pathways in vivo is unclear. Here we used cerebral ischemia/reperfusion as a model to investigate the interaction between apoptosis and necroptosis. We show that the activation of RIPK1 sequentially promotes necroptosis followed by apoptosis in a temporally specific manner. Cerebral ischemia/reperfusion insult rapidly activates necroptosis to promote cerebral hemorrhage and neuroinflammation. *Ripk3* deficiency reduces cerebral hemorrhage and delays the onset of neural damage mediated by inflammation. Reduced cerebral perfusion resulting from arterial occlusion promotes the degradation of TAK1, a suppressor of RIPK1, and the transition from necroptosis to apoptosis. Conditional knockout of TAK1 in microglial/infiltrated macrophages and neuronal lineages sensitizes to ischemic infarction by promoting apoptosis. Taken together, our results demonstrate the critical role of necroptosis in mediating neurovascular damage and hypoperfusion-induced TAK1 loss, which subsequently promotes apoptosis and cerebral pathology in stroke and neurodegeneration.

apoptosis | necroptosis | RIPK1 | RIPK3 | stroke

Stroke is a leading cause of death and serious long-term disability globally. A large body of research has implicated multiple cell death and proinflammatory pathways in mediating neurologic damage in this devastating disease (1). However, we still do not understand the mechanisms that promote the activation of and interaction between different cell death pathways in stroke. Necroptosis and apoptosis are two regulated cell death mechanisms that have been implicated in mediating the neurologic damage in stroke (2, 3). Necroptosis, a form of regulated necrosis, was first demonstrated by the development and application of the small-molecule inhibitor Necrostatin-1 (Nec-1/Nec-1s) in the absence of its targeting mechanism (2). Nec-1s was found to be a highly specific inhibitor of RIPK1 kinase (4). Activation of RIPK1 has been shown to mediate two alternative cell death mechanisms depending on the apoptotic competency of the cell: necroptosis under apoptosis-deficient conditions and apoptosis under apoptosis-proficient conditions (5). TNFα stimulation of cells with caspase inhibition promotes the activation of RIPK1 and its interaction with RIPK3, which in turn phosphorylates MLKL (mixed-lineage kinase domain-like pseudokinase) to mediate the execution of necroptosis (6, 7). Under apoptosis-proficient conditions, TNFα stimulation can lead to the activation of RIPK1 kinase activity to promote RIPK1-dependent apoptosis (RDA) by mediating the formation of complex IIa with FADD and caspase-8 (8, 9). It is unclear in vivo, without the artificial inhibition of caspases, how cells choose to die by necroptosis or apoptosis.

TAK1 (encoded by the gene MAP3K7) is a key mediator of multiple intracellular signaling pathways (10). In TNFα-stimulated cells, TAK1 mediates the phosphorylation of IKK complex to promote activation of the NF-κB pathway. TAK1 also controls the activation of RIPK1, as the loss of TAK1 is highly effective in sensitizing cells to RDA (11). Down-regulation of TAK1 levels in aging human brains has been shown to provide an underlying mechanism that promotes the onset of amyotrophic lateral sclerosis/frontotemporal dementia in individuals with inherited haploinsufficiency of TBK1 (12).

While apoptosis has been shown to transition into necroptosis on inhibition of caspases (2, 7), it is unclear whether necroptosis may also transition into apoptosis and, if so, what conditions may mediate this transition. Here we investigated the activation of necroptosis and apoptosis in the brains of mice subjected to transient middle cerebral artery occlusion (MCAO), a model for stroke in humans. We detected activated RIPK1 (p-S166 RIPK1) in microglia/infiltrated macrophages, neurons, and cerebral endothelial cells in the brains after ischemic insult. Necroptosis was rapidly activated in endothelial cells after a transient ischemic insult at the onset of reperfusion to mediate vascular damage, whereas neurons showed early activation of necroptosis, followed by apoptosis triggered by a reduction in TAK1 level. Selective loss of TAK1 in microglia/infiltrated macrophages and neurons promoted apoptotic neuronal cell death and inflammation. Finally, genetic inhibition of RIPK1 kinase reduced ischemic infarct by blocking both necroptosis and RDA and dampening neuroinflammation, whereas blocking necroptosis alone by RIPK3 deficiency reduced cerebral hemorrhage and long-term ischemic infarct volume.

Significance

Necroptosis has been defined as a regulated cell death mechanism that can be activated under apoptosis deficient conditions. Here we show that necroptosis can be activated under brain ischemic conditions without inhibition of apoptosis. Furthermore, neuronal necroptosis can be followed by delayed apoptosis after the reduction of TAK1 under ischemic conditions. Our study demonstrates the complex interaction of apoptosis and necroptosis after ischemic brain insult and suggests the therapeutic targeting of RIPK1 kinase for the treatment of stroke.

Author contributions: M.G.N. and J.Y. designed research; M.G.N., D.X., P.A., J.L., H.W., and W.L. performed research; M.K. and M.P. contributed new reagents/analytic tools; M.G.N. analyzed data; and M.G.N. and J.Y. wrote the paper.

Reviewers: J.C., University of Pittsburgh; and R.M.F., University of Pittsburgh.

Competing interest statement: J.Y. is a consultant of Denali Therapeutics Inc., which has licensed the necrostatin technology. M.P. received consulting and speaker fees from Genentech, GlaxoSmithKline, Boehringer Ingelheim, and Sanofi. All other authors declare no competing interests.

[1]To whom correspondence may be addressed. Email: junying_yuan@hms.harvard.edu.

This article contains supporting information online at https://www.pnas.org/lookup/suppl/doi:10.1073/pnas.1916427117/-/DCSupplemental.

First published February 18, 2020.

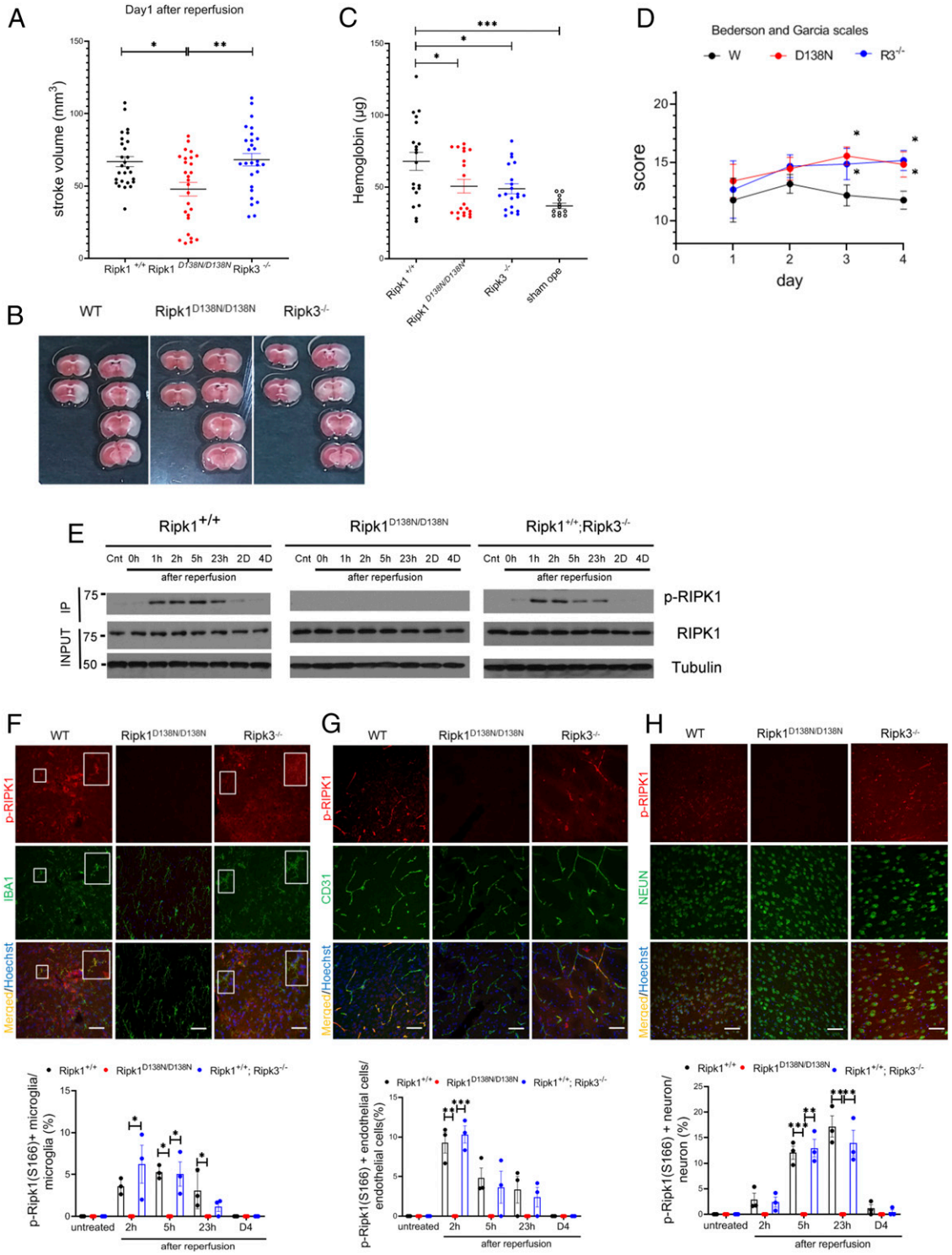

Fig. 1. Activation of RIPK1 by ischemic insult. (*A*) WT, *Ripk1*$^{D138N/D138N}$, and *Ripk3*$^{-/-}$ mice were subjected to transient 60-min MCAO, followed by reperfusion. The mice were killed after 23 h of reperfusion, and the brains were processed for TTC staining to measure infarct volume ($n = 27$ per group). (*B*) Representative TTC stainings from mice subjected to 60 min of ischemia followed by 23 h of reperfusion. (*C*) Quantification of hemorrhagic lesions by hemoglobin quantification in WT, *Ripk1*$^{D138N/D138N}$, and *Ripk3*$^{-/-}$ mice treated as in *A*. (*D*) WT, *Ripk1*$^{D138N/D138N}$, and *Ripk3*$^{-/-}$ mice were subjected to transient 60 min of MCAO followed by reperfusion, and were evaluated with Bederson and Garcia scales in a double-blinded manner daily from day 1 to day 4 after the MCAO procedure ($n = 12$ per group). The highest score is 21 points, and a higher score is correlated with better outcome. (*E*) Brain lysates from mice with indicated genotypes subjected to MCAO for 60 min followed by reperfusion for the indicated time periods were immunoprecipitated with p-S166 RIPK1 and then analyzed by immunoblotting with the indicated antibodies. (*F–H*, *Upper*) Sections of WT, *Ripk1*$^{D138N/D138N}$, and *Ripk3*$^{-/-}$ mice treated with transient 60 min of MCAO followed by reperfusion for 23 h (*F* and *H*) or 3 h (*G*) and at different time points as indicated on the bar graphs were immunostained with p-S166 RIPK1 and coimmunostained with IBA1, CD31, or NeuN for IBA1^{+} microglia/infiltrated macrophages (*F*), cerebrovascular endothelial cells (*G*), and neurons (*H*), respectively. (Magnification: 40×; Sale bar: 50 μm.) (*F–H*, *Lower*) The quantification of the results. The data represent mean ± SEM. $n = 3$ mice for each time point. Assessment of each time point includes data from five sections for approximately 150 cells in each mouse. (*F*) The large square *Insets* (*Right*) are enlarged images of the small square *Insets* (*Left*). $^{*}P < 0.05$, $^{**}P < 0.01$, and $^{***}P < 0.001$.

Results

Genetic and Pharmacologic Inhibition of RIPK1 Reduces Ischemic Brain Injury. To explore the cell death mechanisms in stroke, wild-type (WT) mice, *Ripk1*$^{D138N/D138N}$ mice carrying a RIPK1 kinase dead knockin allele D138N, and *Ripk3*$^{-/-}$ mice were subjected to transient MCAO, a mouse model for stroke, with 60 min of occlusion followed by 23 h of reperfusion (2). The extent of cerebral infarction was measured at 24 h after the onset of MCAO. The stroke volume in *Ripk1*$^{D138N/D138N}$ mice, but not in *Ripk3*$^{-/-}$ mice, was significantly reduced compared with WT mice when analyzed at 24 h after MCAO (Fig. 1 *A* and *B*).

Intracerebral hemorrhage is one of the most common types of stroke in humans (13). Accordingly, we analyzed whether blocking necroptosis impacted hemorrhagic transformation in the MCAO model. We found that the incidence of hemorrhagic transformation induced by MCAO was significantly lower in both *Ripk1*$^{D138N/D13N8}$ mice and *Ripk3*$^{-/-}$ mice relative to WT controls (Fig. 1*C* and Fig. S1*A*). Stroke volumes were smaller in both *Ripk1*$^{D138N/D13N8}$ mice and *Ripk3*$^{-/-}$ mice compared with WT mice on day 4 after MCAO, which may include the effect of infiltrating immune cells at late time points (*SI Appendix*, Fig. S1*B*). Improvements in behavior scores were greater in both *Ripk1*$^{D138N/D13N8}$ mice and *Ripk3*$^{-/-}$ mice compared with WT mice (Fig. 1*D*). These results suggest that necroptosis is important for mediating vascular pathology to promote ischemic infarct, and that the activation of RIPK1 may mediate deleterious events beyond activating RIPK3-driven necroptosis. Thus, inhibition of RIPK1 may be more effective than RIPK3 deficiency in protecting against cerebral ischemic infarction.

To investigate the interaction of RIPK1 and RIPK3 in mediating cerebral ischemic injury, we assessed the activation of RIPK1 after ischemic insult by immunoblotting using p-S166 RIPK1, a biomarker of RIPK1 activation (12, 14). We found that RIPK1 was rapidly activated at 1 h after the onset of reperfusion in WT mice, and the activation of RIPK1 was blocked in *Ripk1*$^{D138N/D13N8}$ mice but not in *Ripk3*$^{-/-}$ mice (Fig. 1*E*). This result suggests that RIPK1 is activated upstream of RIPK3 after ischemic insult.

We next characterized the cell types with activated RIPK1 after MCAO induction by immunostaining. p-S166 RIPK1 signal was found in IBA1$^+$ microglia/infiltrated macrophages, endothelial cells, and neurons in the penumbra area of the cortex in WT mice subjected to MCAO. The p-S166 RIPK1 immunostaining showed distinct time courses in these three cell types: CD31$^+$ endothelial cells and IBA1$^+$ microglia/infiltrated macrophages showed a peak in p-S166 RIPK1$^+$ at 2 h after reperfusion, while NeuN$^+$ neurons began to show p-S166 RIPK1$^+$ at ∼2 to 5 h after reperfusion, with a peak around 23 h (Fig. 1 *F*–*H*). Increases in p-S166 RIPK1$^+$ were completely blocked by genetic inhibition of RIPK1 in *Ripk1*$^{D138N/D138N}$ mice, while the loss of RIPK3 in *Ripk3*$^{-/-}$ mice had no effect on the activation of RIPK1.

We also performed immunostaining to assess total RIPK1 levels on brain sections of sham-operated mice and MCAO mice. In sham-operated mouse brains, RIPK1 signals were detected predominately in IBA1$^+$ microglia and CD31$^+$ endothelial cells (*SI Appendix*, Fig. S2*A*). After MCAO induction in WT or *Ripk3*$^{-/-}$ animals, we found increased RIPK1$^+$IBA1$^+$ microglia/infiltrated macrophages, RIPK1$^+$CD31$^+$ endothelial cells, and RIPK1$^+$NeuN$^+$ neurons (*SI Appendix*, Fig. S2 *C* and *D*). Interestingly, the levels of Ripk1 mRNA or protein were not increased in the brains of WT mice over the course of ischemic insult, nor did *Ripk1*$^{D138N/D138N}$ or *Ripk3*$^{-/-}$ have any effect (*SI Appendix*, Fig. S2 *E* and *F*). Thus, the apparent increases in RIPK1$^+$ cells detected in brains after ischemic insult are likely due to a conformational change in RIPK1 during its activation.

Collectively, these results demonstrate that the kinase activity of RIPK1 is promoted by cerebral ischemic insult. Furthermore, they show that genetic or pharmacologic inhibition of RIPK1 kinase can reduce stroke volume, and while the loss of RIPK3 has no effect on RIPK1 activation, blocking necroptosis by Ripk3$^{-/-}$ can reduce the risk of intracerebral hemorrhage and stroke volume at later time points.

Activation of Necroptosis and Apoptosis after Ischemic Insult. Since RIPK1 kinase activity is activated by cerebral ischemic brain insult, we next examined two major downstream cell death pathways mediated by activated RIPK1: necroptosis and RDA. Necroptosis can be activated under apoptosis-deficient conditions. In necroptosis, activated RIPK1 interacts with RIPK3 to promote its activation, which is marked by p-T231/S232 RIPK3. Activated RIPK3 in turn phosphorylates MLKL, marked by p-S345 MLKL, to mediate the execution of necroptosis (7, 15–17). Activated RIPK3 and MLKL exhibit differential solubility relative to a control state and become concentrated in a Nonidet P-40 insoluble 6 M urea fraction (14, 18). On immunoblot analysis of brain lysates from WT mice after ischemic insult, p-T231/S232 RIPK3 and p-S345 MLKL were detected immediately on reperfusion and remained elevated until ∼5 h after the onset of reperfusion (Fig. 2*A*). Reperfusion after ischemic occlusion is essential for the activation of necroptosis, as p-MLKL was not detected in the ischemic brains without reperfusion (a permanent occlusion stroke model) (Fig. 2 *B* and *C*). In addition to necroptosis, the cleavage of caspase-3, the biomarker of apoptosis, was also detected in ischemic brains, peaking at 24 h after the ischemic insult (Fig. 2*A*).

We also analyzed p-S345 MLKL and p-T231/S232 RIPK3 by immunostaining. Both p-S345 MLKL and p-T231/S232 RIPK3 were found to be coimmunostained with CD31$^+$ endothelial cells within 2 h after the onset of reperfusion in the penumbra area of the cortex (Fig. 2 *D* and *E*). This suggests that a substantial proportion of the necroptotic cell death occurring after ischemic brain insult is in endothelial cells.

We also detected p-S345 MLKL and p-T231/S232 RIPK3 in neurons after MCAO (Fig. 2 *F* and *G*). In addition to the hallmarks of necroptosis, we also found a substantial portion of NeuN$^+$ neurons that had cleaved caspase-3$^+$ (CC3$^+$), which occurred in a delayed fashion relative to necroptosis (Fig. 2*H*). Thus, a cerebral ischemic insult in WT mice triggers necroptosis in endothelial cells immediately after the onset of reperfusion, which contributes to intracerebral hemorrhage, while neurons may undergo both necroptosis and apoptosis.

MCAO-induced p-T231/S232 RIPK3 and p-S345 MLKL signals were suppressed in both *Ripk1*$^{D138N/D138N}$ and *Ripk3*$^{-/-}$ mice (Fig. 2 *D*–*G*). In contrast, the cleavage of caspase-3 was suppressed only in *Ripk1*$^{D138N/D138N}$ mice, not in *Ripk3*$^{-/-}$ mice (Fig. 2*H*). This suggests that cerebral ischemic insult also triggers RDA.

Since cerebral inflammation plays an important role in the outcome of stroke (19), and both necroptosis and RDA promote inflammation (20), we next characterized the impact of inhibiting RIPK1 kinase and RIPK3 loss on IBA1$^+$ microglia/infiltrated macrophages, major mediators of neuroinflammation. We characterized the number and morphology of microglia/infiltrated macrophages in the brains of WT, *Ripk1*$^{D138N/D138N}$, and *Ripk3*$^{-/-}$ mice after ischemic insult at different time points after the onset of reperfusion. We observed no significant difference in the numbers of microglia/infiltrated macrophages between three groups; however, microgliosis with activated amoeboid-like microglia/infiltrated macrophages was suppressed in the brains of *Ripk1*$^{D138N/D138N}$, but not *Ripk3*$^{-/-}$, mice (*SI Appendix*, Fig. S3 *A*–*C*).

We also used quantitative RT-PCR to measure the mRNA expression of proinflammatory cytokines and chemokines in the brains of MCAO-induced WT, *Ripk1*$^{D138N/D138N}$, and *Ripk3*$^{-/-}$ mice at different time points after the onset of reperfusion. We observed decreased levels of proinflammatory cytokines

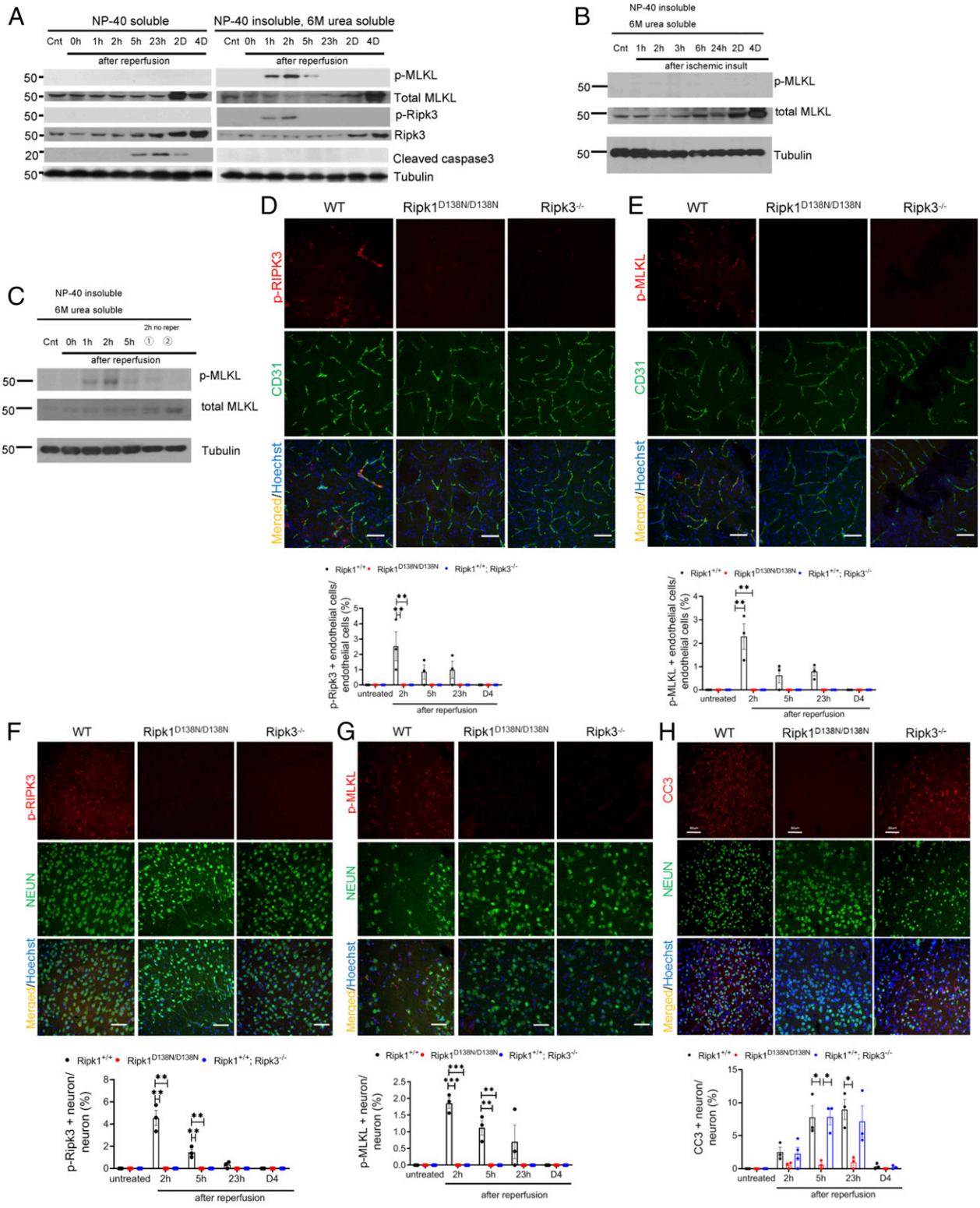

Fig. 2. Activation of necroptosis and apoptosis by ischemic insult. (*A*) Brain lysates from WT mice treated with MCAO for 60 min, followed by reperfusion for the indicated time periods were analyzed by immunoblotting for p-S345 MLKL, MLKL, p-T231/S232 RIPK3, RIPK3, CC3, and Tubulin. (*B*) Brain lysates from WT mice treated with permanent occlusion for the indicated time periods were analyzed by immunoblotting for p-S345 MLKL, MLKL, and Tubulin. (*C*) Brain lysates prepared in 6 M urea from WT mice treated with MCAO for 60 min followed by reperfusion for 0, 1, 2, or 5 h or without reperfusion were analyzed by immunoblotting for p-S345 MLKL and MLKL. (*D–E*, *Upper*) Brain sections of WT, *Ripk1*$^{D138N/D138N}$, and *Ripk3*$^{-/-}$ mice treated with MCAO for 60 min followed by reperfusion for 3 h were immunostained for p-T231/S232 RIPK3 (*D*) and p-S345 MLKL (*E*) and coimmunostained with CD31. P-RIPK3^{+} endothelial cells at different time points were quantified (*Bottom*). (*F–H*) Brain sections of WT, *Ripk1*$^{D138N/D138N}$, and *Ripk3*$^{-/-}$ mice treated with MCAO for 60 min followed by reperfusion for 23 h were immunostained for p-T231/S232 RIPK3 (*F*), p-S345 MLKL (*G*), or CC3 (*H*) and coimmunostained with NeuN. (*D–H*, *Lower*) P-RIPK3^{+}, p-MLKL^{+}, and CC3^{+} neurons or endothelial cells as indicated at different time points were quantified. The data represent mean ± SEM; n= 3 mice per time point. (Magnification: 40×; Scale bar: 50 μm.) Assessment of each time point includes data from five sections for approximately 150 cells from each mouse. *$P < 0.05$, **$P < 0.01$, and ***$P < 0.001$.

and chemokines, including TNFα, IL6, IL1α, IL1β, and Cxcl1, in the brains of *Ripk1*$^{D138N/D138N}$ mice during reperfusion after ischemic insult (Fig. 3). In contrast, the pattern of proinflammatory cytokine and chemokine expression in the brains of *Ripk3*$^{-/-}$ mice was similar to that of WT mice, with a slight decline at the 23-h timepoint. These results suggest that a RIPK1 kinase-mediated inflammatory response is activated early after the ischemic insult, while necroptosis mediated by RIPK3 can also contribute to inflammation in a time-delayed manner.

Taken together, the foregoing results demonstrate that necroptosis is activated rapidly in endothelial cells and neurons after cerebral ischemia-reperfusion, while RDA is induced in neurons in a delayed fashion, peaking at ∼24 h after ischemic insult and reperfusion. Since RIPK1 kinase is involved in mediating necroptosis, RDA, and inflammation, inhibition of RIPK1 kinase can block the death of endothelial cells and neurons, as well as the production of proinflammatory cytokines and chemokines, while blocking necroptosis may only partially rescue cell death and amplification of the inflammatory response after the onset of reperfusion.

Reduction of TAK1 after Ischemic Insult. We next examined the mechanisms promoting apoptosis during reperfusion after ischemic insult. Since TAK1 is an important negative regulator of RDA (11), we assessed whether loss of TAK1-mediated suppression was involved by examining its expression levels in the brains of WT mice during reperfusion after ischemic insult. Interestingly, we found that the levels of TAK1 started to decrease during reperfusion at ∼2 h after the ischemic insult (Fig. 4*A*). Phosphorylation of Thr180/Thy182 p38 and Thy183/Tyr185 JNK, the downstream substrates of TAK1, were also reduced during reperfusion around the same time period, while phosphorylation of Thr202/Thr204 ERK showed no difference. A similar reduction in the levels of TAK1 protein was observed in the brains of WT, *Ripk1*$^{D138N/D138N}$, and *Ripk3*$^{-/-}$ mice during reperfusion after ischemic insult (Fig. 4*B*). Thus, the loss of TAK1 is likely to be upstream and independent of RIPK1 and RIPK3.

We also assessed the cell types that showed reduced TAK1 expression in the brains of WT mice by immunostaining. In sham-operated WT brains, TAK1 was expressed by both IBA1^{+} microglia/infiltrated macrophages and NeuN^{+} neurons.

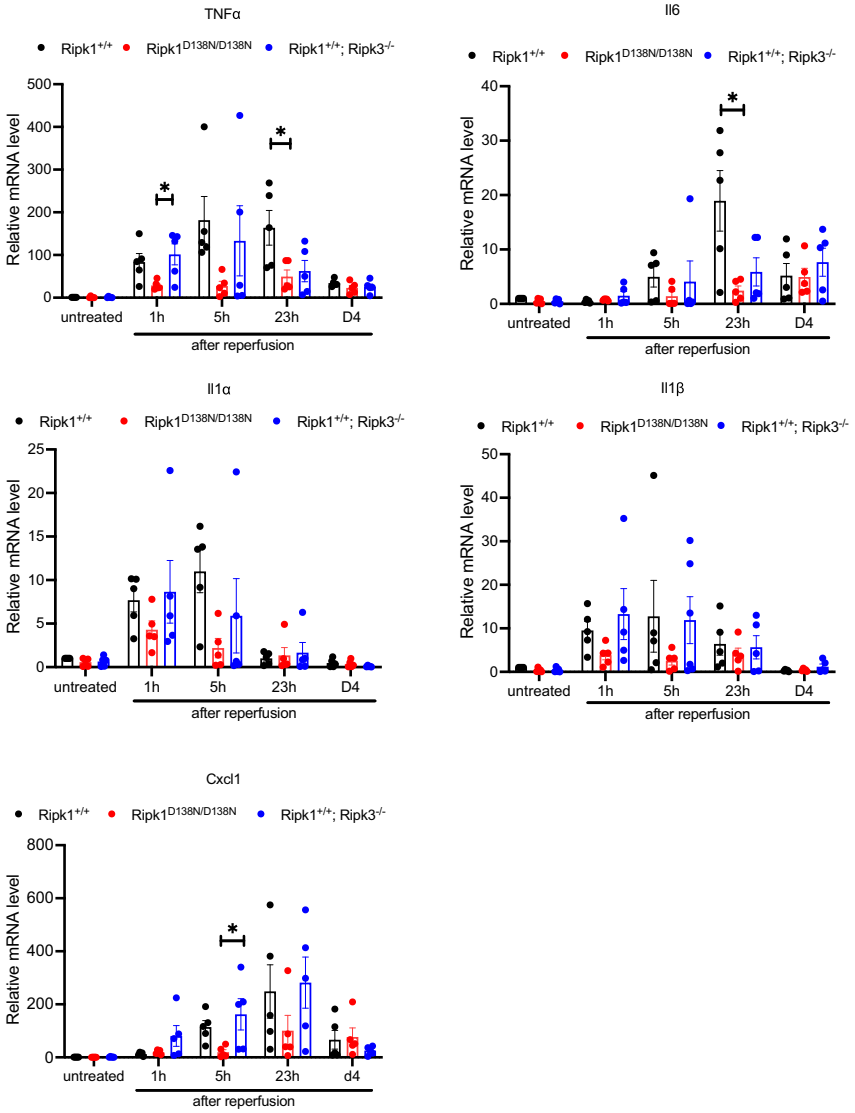

Fig. 3. Inhibition of RIPK1 blocks neuroinflammation induced by cerebral ischemic insult. Quantitative RT-PCR analysis of the mRNA expression levels of indicated cytokines and chemokines in the brain lysates from WT, *Ripk1*$^{D138N/D138N}$, and *Ripk3*$^{-/-}$ mice treated with MCAO for 60 min followed by reperfusion for the indicated time periods (n = 5 mice for each time point). The data represent mean ± SEM. *$P < 0.05$.

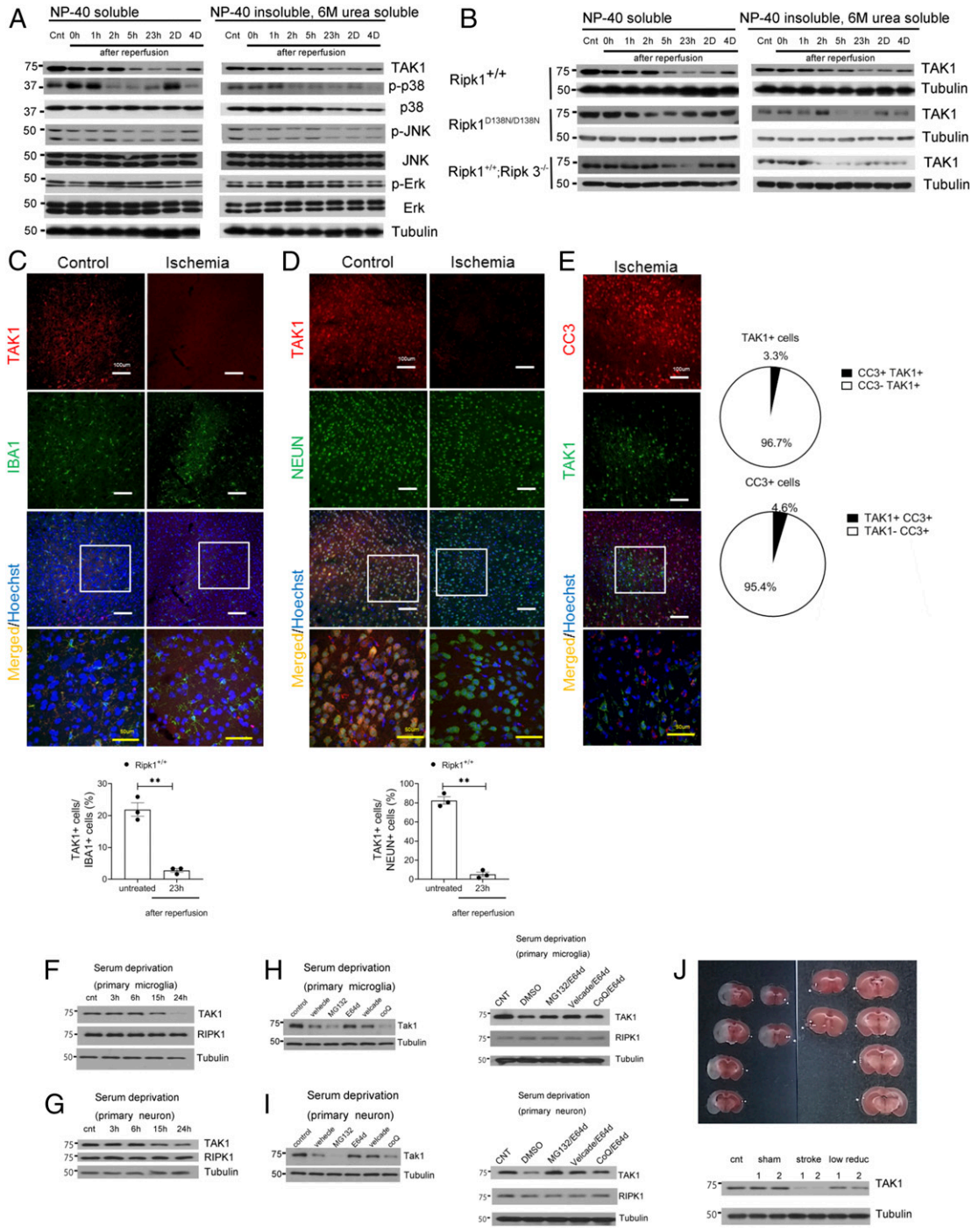

Fig. 4. Reduction of TAK1 in neurons and microglia/infiltrated macrophages induced by cerebral hypoperfusion. (*A*) Brain lysates from WT mice treated with MCAO for 60 min followed by reperfusion for the indicated time periods were analyzed by immunoblotting for TAK1, p-(T180/Y182) p38, p38, p-T183/Y185 JNK, JNK, p-T202/Y204 ERK, and ERK, with Tubulin as a loading control. (*B*) Brain lysates from mice with indicated genotypes subjected to MCAO for 60 min followed by reperfusion for the indicated time periods were analyzed by immunoblotting for TAK1 and Tubulin as a loading control. The same WT Ripk1$^{+/+}$ data in *A* were used in *B* to compare with that of mutant mice. (*C* and *D*, *Upper*) Brain sections from WT mice subjected to MCAO for 60 min followed by reperfusion for 23 h were immunostained with TAK1 and coimmunostained with IBA1 (*C*) and NeuN (*D*). The nuclei were stained by Hoechst stain. Quantification of TAK1^{+}/IBA1^{+} microglia/infiltrated macrophages and TAK1^{+}/NeuN^{+} neurons are shown at the bottom of each panel. $n = 3$ mice. Quantifications include about 100 TAK1^{+} cells and about 100 CC3^{+} cells from each mouse. The fourth panels in each column are enlarged images of the *Insets*. (Scale bar, white: 100 μm; Magnification: 20×.) (Scale bar, yellow: 50 μm; Magnification: 40×.) (*E*, *Left*) TAK1^{+}/CC3^{+} cells at 24 h after MCAO were quantified by double immunostaining for TAK1 and CC3. $n = 3$ mice. (*E*, *Right*) Quantifications included ∼100 cells. The data represent mean ± SEM. The fourth panels in each column are enlarged images of the *Insets*. (Scale bar, white: 100 μm; Magnification: 20×.) (Scale bar, yellow: 50 μm; Magnification: 40×.) (*F*–*I*) Primary microglia (*F* and *H*) and neurons (*G* and *I*) from WT mice were treated with serum deprivation in the presence of MG132 (10 μM), E64d (5 μg/mL), Velcade (50 ng/mL), chloroquine (50 μg/mL), or a combination as indicated for 18 h. The lysates were analyzed by immunoblotting for TAK1, RIPK1, and Tubulin. (*J*) TTC staining of the mice with >80% rCBF reduction (*Left*) and <80% rCBF reduction (*Right*). Brain lysates from WT mice treated with no operation, sham operation, MCAO with >80% rCBF reduction, and MCAO with <80% rCBF reduction followed by reperfusion for 23 h were analyzed by immunoblotting for TAK1 and Tubulin as a loading control. *$P < 0.05$, **$P < 0.01$, and ***$P < 0.001$.

TAK1 levels were reduced in both microglia/infiltrated macrophages and neurons at 23 h of reperfusion after ischemic insult (Fig. 4 *C* and *D*). Consistent with suppression of apoptosis by TAK1, we found that the presence of activated $CC3^+$ was largely excluded from cells that were positive for TAK1 expression (Fig. 4*E*). No reduction of MAP3K7 mRNA was detected after ischemic insult and reperfusion in WT, $Ripk1^{D138N/D138N}$, or $Ripk3^{-/-}$ animals, suggesting that the loss of TAK1 expression is unlikely to be the result of reduced transcription (*SI Appendix*, Fig. S4).

We have previously reported the reduction of TAK1 expression in aging human brains (12) and aging has also been shown to lead to declined blood perfusion of tissues and organs (21). Thus, we considered whether hypoperfusion may be a common contributing factor reducing TAK1 levels in stroke and aging brains. Indeed, we found that serum removal reduced the levels of TAK1 in cultured primary microglia and neurons (Fig. 4 *F* and *G*). Inhibition of proteasomal and lysosomal degradation simultaneously, but not individually, blocked the reduction of TAK1 from neurons and microglia under serum removal conditions, suggesting both lysosomal and proteasomal degradation of TAK1 can occur (Fig. 4 *H* and *I*). Similarly, removing serum from cultured murine embryonic fibroblasts (MEFs) also reduced the levels of TAK1, which could be rescued by blocking both proteasomal and lysosomal degradation by MG132/E64d or Velcade/E64d (*SI Appendix*, Fig. S5 *A* and *B*). Levels of MAP3K7 mRNA were even slightly increased in MEFs on serum removal, confirming that the reduction of TAK1 is not mediated by changes in transcription (*SI Appendix*, Fig. S5*C*). In contrast, the levels of total RIPK1 were not altered by serum withdrawal, aligned to the supposition that TAK1 alterations are upstream of RIPK1.

To examine the effects of hypoperfusion in vivo, we analyzed the brains of mice in which MCAO was induced, but regional cerebral blood flow (rCBF) was reduced by <80%, which was not sufficient to induce stroke. Interestingly, a reduction in TAK1 levels was found in these mouse brains, which did not show infarction (Fig. 4*J*). Thus, even a mild rCBF reduction can lead to a TAK1 reduction in vivo, which may serve as a useful paradigm to understand TAK1 reductions in the aging brain. These results suggest that reduction of blood perfusion in the brains after stroke is sufficient to reduce the levels of TAK1 by promoting its degradation.

Reduction of TAK1 Promotes Apoptosis after Ischemic Brain Insult. To understand the functional significance of TAK1 reduction in ischemic brains, we selectively reduced the expression of TAK1 in the myeloid or neuronal lineages by generating conditional $MAP3K7^{fl/fl}$; $Lyz2^{cre/+}$ or $MAP3K7^{fl/fl}$; $Emx^{cre/+}$ mice, respectively. We have confirmed TAK1 deletion in these conditional knockout mice (*SI Appendix*, Fig. S6*A*). The reduction of TAK1 from either a myeloid or a neuronal lineage led to an increase in stroke volume compared with that of WT mice (Fig. 5*A*). We assessed the impact of TAK1 reduction on RIPK1 activation after ischemic insult using immunoblotting of p-S166 RIPK1 and found that p-S166 RIPK1 was increased and persisted longer after MCAO in the $MAP3K7^{fl/fl}$; $Lyz2^{cre/+}$ or $MAP3K7^{fl/fl}$; $Emx^{cre/+}$ mice compared with WT mice (Fig. 5*B*). The signal of p-S166 RIPK1 remained detectable in the $MAP3K7^{fl/fl}$; $Emx^{cre/+}$ mice at 4 d after MCAO, when it was below the limit of detection in WT mice.

We next performed p-S166 RIPK1 immunostaining in the brains of WT, $MAP3K7^{fl/fl}$; $Lyz2^{cre/+}$, and $MAP3K7^{fl/fl}$; $Emx^{cre/+}$ mice following MCAO. The percentage of p-S166 $RIPK1^+$ $IBA1^+$ microglia/infiltrated macrophages was higher in $MAP3K7^{fl/fl}$; $Lyz2^{cre/+}$ mice compared with WT or $MAP3K7^{fl/fl}$; $Emx^{cre/+}$ mice at 2 to 5 h after reperfusion (Fig. 5*C*). $CD31^+$ endothelial cells showed similar percentages of p-S166 $RIPK1^+$ cells in all three types of mice (Fig. 5*D*). $MAP3K7^{fl/fl}$; $Lyz2^{cre/+}$ mice had a higher percentage of p-S166 $RIPK1^+$ $NeuN^+$ neurons at 2 to 5 h after reperfusion compared with WT and $MAP3K7^{fl/fl}$; $Emx^{cre/+}$ mice; while $MAP3K7^{fl/fl}$; $Emx^{cre/+}$ mice had a higher percentage of p-S166 $RIPK1^+$ neurons on day 4 (Fig. 5*E*). These results suggest that TAK1 deficiency promotes the activation of RIPK1 in both microglia/infiltrated macrophages and neurons with distinct time courses.

We next analyzed the consequences of TAK1 deficiency on the induction of apoptosis after cerebral ischemic insult. In $MAP3K7^{fl/fl}$; $Lyz2^{cre/+}$ mice, cerebral ischemia-mediated CC3 occurred earlier than in WT mice and was detectable as early as 2 h after the onset of reperfusion; in addition, the peak of CC3 was earlier relative to that in WT mice (Fig. 6 *A* and *B*). This suggests that neuronal apoptosis can be induced by TAK1-deficient microglia/infiltrated macrophages in a non–cell-autonomous fashion. This bystander effect of microglia/infiltrated macrophages is likely mediated by cytokine and chemokine production, as levels of proinflammatory cytokines, such as TNFα and IL6, were higher in the brains of $MAP3K7^{fl/fl}$; $Lyz2^{cre/+}$ mice relative to WT mice at 5 h after reperfusion (Fig. 6*C*).

In $MAP3K7^{fl/fl}$; $Emx^{cre/+}$ mice, the onset of CC3 was not altered compared with that in WT mice; however, maximal CC3 occurred earlier and in greater magnitude relative to WT, and CC3 was still detected in $MAP3K7^{fl/fl}$; $Emx^{cre/+}$ mice, but not in WT mice, at 4 d after ischemic insult (Fig. 6*B*).

The loss of TAK1 from either the myeloid or neuronal lineage did not significantly affect the activation of necroptosis induced by cerebral ischemia as measured by p-MLKL levels in brain lysates from both $MAP3K7^{fl/fl}$; $Lyz2^{cre/+}$ mice and $MAP3K7^{fl/fl}$; $Emx^{cre/+}$ mice subjected to MCAO (*SI Appendix*, Fig. S6 *B*–*F*).

In addition to increased levels of apoptosis, we found significant increases in the levels of proinflammatory cytokines and chemokines in both $MAP3K7^{fl/fl}$; $Lyz2^{cre/+}$ mice and $MAP3K7^{fl/fl}$; $Emx^{cre/+}$ mice subjected to MCAO (Fig. 6*C*). In $MAP3K7^{fl/fl}$; $Lyz2^{cre/+}$ mice treated with MCAO, the levels of proinflammatory cytokines were higher than those in WT mice at 5 h after reperfusion, while in $MAP3K7^{fl/fl}$; $Emx^{cre/+}$ mice, proinflammatory cytokine levels were similar to those in WT in this early period. However, from 24 h to day 4 after reperfusion, $MAP3K7^{fl/fl}$; $Emx^{cre/+}$ mice showed augmented levels of proinflammatory cytokines, suggesting that sustained apoptosis after the loss of TAK1 from neurons can also promote the production of proinflammatory signals.

To investigate whether the activation of apoptosis on TAK1 loss is dependent on RIPK1 kinase function, we administered a specific inhibitor of RIPK1 kinase, Nec-1s, to both $MAP3K7^{fl/fl}$; $Lyz2^{cre/+}$ mice and $MAP3K7^{fl/fl}$; $Emx^{cre/+}$ mice that had been subjected to MCAO. The administration of Nec-1s suppressed cleavage of caspase-3 in both types of mice (Fig. 6 *D* and *E*).

Collectively, these findings suggest that reduced expression of TAK1 in microglia/infiltrated macrophages promotes the production of proinflammatory cytokines, which in turn activates neuronal apoptosis non–cell-autonomously. In addition, selective loss of TAK1 from neurons augments apoptosis in both magnitude and temporal duration, as well as the production of proinflammatory cytokines. Taken together, these results suggest that the reduction of TAK1 in postischemic brains promotes apoptosis and neuroinflammation.

Discussion

In this study, we examined the temporal and interactive relationship between necroptosis and apoptosis after ischemic brain insult and found that necroptosis is rapidly activated after cerebral ischemic insult in a reperfusion-dependent manner. Based on the biomarkers of necroptosis, p-RIPK3 and p-MLKL, necroptosis induced by ischemic insult occurs primarily in cerebral endothelial cells and neurons, while apoptosis occurs primarily in neurons in a time-delayed fashion. Activated microglia/infiltrated macrophages after ischemic insult show p-RIPK1, supporting the role of RIPK1 in mediating neuroinflammation

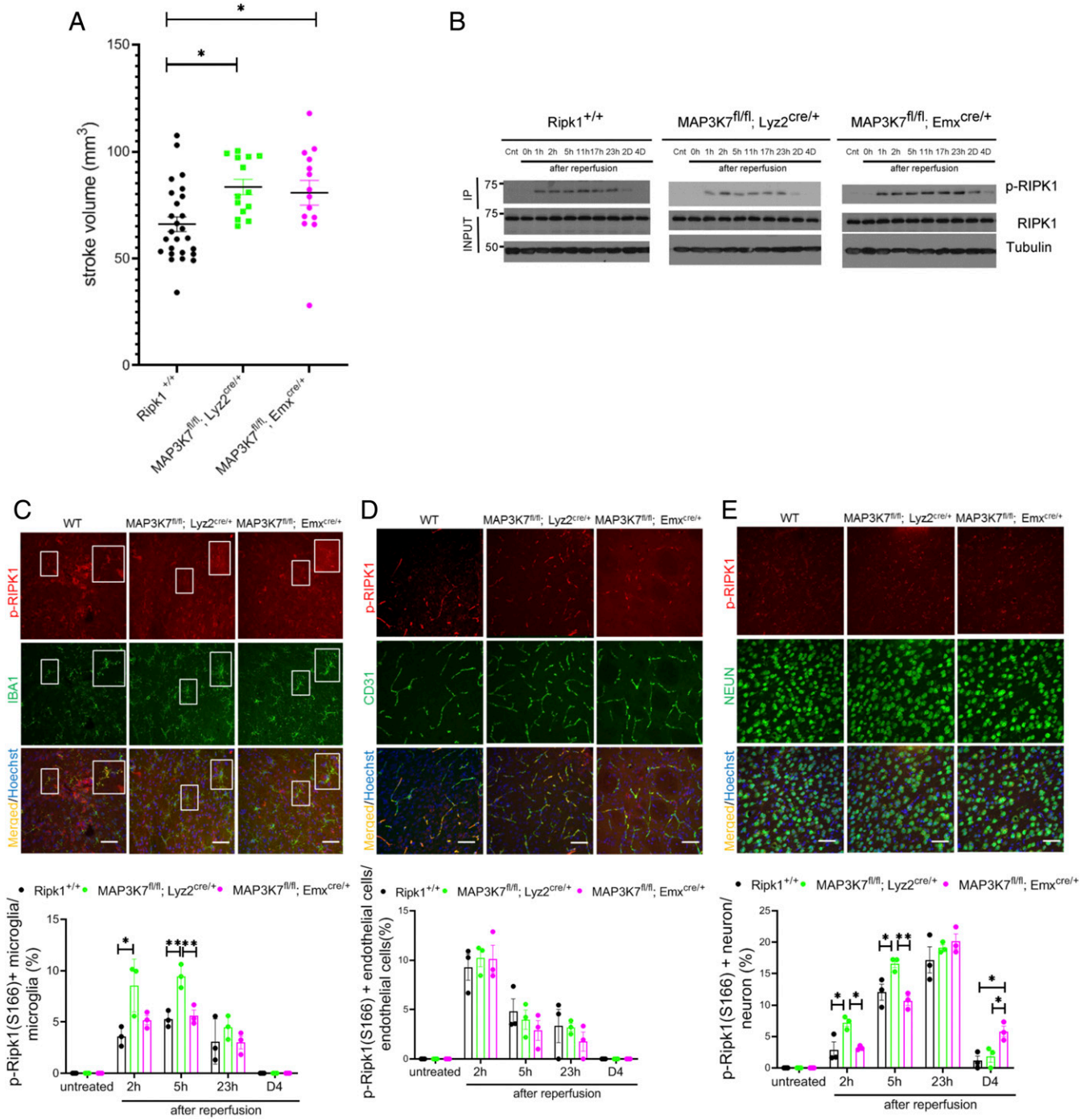

Fig. 5. Selective TAK1 loss augments the activation of RIPK1 to promote apoptosis. (*A*) WT, *MAP3K7*$^{fl/fl}$; *Lyz2*$^{cre/+}$, and *MAP3K7*$^{fl/fl}$; *Emx*$^{cre/+}$ mice (each dot representing 1 mouse) were subjected to transient 60 min of MCAO, followed by reperfusion for 23 h. The brains were processed for TTC staining to measure infarct volume. (*B*) Brain lysates from mice with the indicated genotypes subjected to MCAO for 60 min followed by reperfusion for the indicated time periods were immunoprecipitated with p-S166 RIPK1 and analyzed by immunoblotting with the indicated antibody. (*C–E*, *Upper*) Sections of WT, *MAP3K7*$^{fl/fl}$; *Lyz2*$^{cre/+}$, and *MAP3K7*$^{fl/fl}$; *Emx*$^{cre/+}$ mice treated with transient 60 min of MCAO followed by reperfusion for 5 h (*C* and *E*) or 3 h (*D*) at different time points as indicated on the bar graphs were immunostained with p-S166 RIPK1 and coimmunostained with IBA1, CD31, or NeuN for microglia/infiltrated macrophages (*C*), cerebrovascular endothelial cells (*D*), and neurons (*E*), respectively. The larger *Insets* (*Right*) in *C* are an enlarged image of the smaller *Insets* (*Left*). (Magnification: 40×; Scale bar: 50 μm.) (*C–E*, *Lower*) The quantification of the results. The data represent mean ± SEM. The quantifications of p-S166 Ripk1^{+} microglia/infiltrated macrophages, endothelial cells, and neurons are shown at the bottom of each panel. $n = 3$ mice for each time point. Assessment of each time point includes data from five sections for approximately 150 cells in each mouse. *$P < 0.05$ and **$P < 0.01$.

(20). We show that necroptosis of cerebral endothelial cells mediates intracerebral hemorrhage. Since neurons undergo both necroptosis and RDA, inhibition of RIPK1 kinase by D138N mutation and Nec-1s, which can block both necroptosis and RDA, reduces the stroke volume, while inhibition of necroptosis by Ripk3$^{-/-}$ rescues cerebral hemorrhage and inflammation, leading to a reduction in ischemic stroke volume only at later timepoints. These results suggest that the activation of RIPK1 is

one of the primary deleterious mechanisms in the brain following ischemic insult. The downstream consequences of RIPK1 activation exhibit cell-type specificity: the activation of RIPK1 in endothelial cells promotes necroptosis and cerebromicrovascular damage, the activation of RIPK1 in neurons promotes both necroptosis and apoptosis at varying timepoints, while the activation of RIPK1 in microglia/infiltrated macrophages promotes inflammation. Since neuronal expression of TNFR1 and TNFR2 is very low under normal conditions (22, 23), our study also suggests the possibility that the activation of RIPK1 in neurons after cerebral ischemia may occur independent of TNFα signaling, raising the question as to how RIPK1 may be activated independent of TNFR1, which is a highly established paradigm in which RIPK1 plays an important role in mediating deleterious signaling responses.

Intracerebroventricular administration of Nec-1 was shown to reduce the infarct volume in MCAO, with an extended time window for neuroprotection (2). Subsequent studies supported the protective effect of inhibiting RIPK1 kinase in ischemic injuries induced in multiple tissues/organs, including brain, eye, heart, and kidney (24–31). While these studies highlighted the important role of RIPK1 as a central mediator of brain damage following acute ischemic neuronal injury, how the activation of RIPK1 mediates tissue injuries and cell death remains unclear. Here we show that the activation of RIPK1 is critical for mediating both apoptosis and necroptosis after ischemic injury, whereas RIPK3-mediated necroptosis primarily mediates vascular pathology and long-term stroke volume. The loss of TAK1 after reduction of cerebral perfusion sensitizes to apoptosis and the transition from necroptosis to RDA.

Our study demonstrates that the mechanism of transition from necroptosis to apoptosis in vivo is mediated by the reduction of TAK1 by hypoperfusion. Apoptosis can be switched to necroptosis on inhibition of caspases (2, 7), but a switch from necroptosis to apoptosis has not been shown. We found that a reduction of TAK1 promotes apoptosis after the activation of necroptosis driven by hypoperfusion. Our results suggest that the reduction of TAK1 in aging human brains (12) might also be attributable to cerebral hypoperfusion. Conditional loss of TAK1 specifically from cells of myeloid lineage, including microglia and macrophages, in $MAP3K7^{fl/fl}$; $Lyz2^{cre/+}$ mice accelerates the onset of apoptosis after ischemic brain insult. Since the activated caspase-3 is present primarily in neurons of WT mice subjected to MCAO, these results suggest that the loss of TAK1 might accelerate the onset of neuronal apoptosis non–cell-autonomously. In addition, since the neuronal-specific loss of TAK1 in $MAP3K7^{fl/fl}$; $Emx^{cre/+}$ mice can promote the magnitude and persistence of apoptosis, this result suggests that the loss of TAK1 can also promote cell-autonomous neuronal apoptosis. Thus, our findings suggest that TAK1 level serves as a critical factor for determining the vulnerability of CNS after ischemic insult. In this regard, the reduced levels of TAK1 in aging human brains (12) may predispose older individuals to cognitive damage mediated primarily by RDA after ischemic stroke, while in younger individuals, stroke may activate primarily necroptosis followed by RDA. This may serve as a future direction for this work.

Activation of proteasomal and lysosomal proteases has been proposed to mediate ischemic brain injury (32–34). Elevated levels of ubiquitin-protein conjugates are observed after cerebral ischemia, which is consistent with the activation of proteasomal degradation (35). Modulation of the ubiquitin-proteasome-system, such as through the administration of proteasomal inhibitors, has been shown to improve neurologic outcomes after cerebral ischemia (36). Here we show that the activation of both proteasomal and lysosomal degradation under ischemic condition is involved in mediating the degradation of TAK1 to sensitize to apoptosis, and thus that reduced TAK1 levels may provide a molecular mechanism that connects the activation of proteasomal and lysosomal systems under ischemic conditions to the onset of apoptosis.

The role of RIPK1 kinase in mediating both cerebral hemorrhage and neuronal cell death in stroke suggests the effectiveness of RIPK1 inhibitors in treating both hemorrhagic and ischemic stroke. Tissue plasminogen activator and mechanical thrombectomy, the approved treatment options for acute ischemic stroke, have intracranial hemorrhage as a common adverse event, and thus are inappropriate for hemorrhagic transformation patients. The current treatment paradigm requires a differential diagnosis between ischemic and hemorrhagic transformation stroke, leading to delays in starting treatment and diminished patient outcomes. Our findings indicate that inhibition of RIPK1 can reduce both hemorrhagic transformation and neuronal cell death, which may allow for the use of RIPK1-targeting therapeutics without a differential diagnosis. Given the large therapeutic window of RIPK1 inhibition (up to 6 h) (2, 3), this may provide an important opportunity to reduce the loss of neurologic function in stroke patients. We demonstrate that the activation of necroptosis depends on reperfusion and is activated immediately after ischemic insult on reperfusion. Endothelial cells, which compose the blood-brain barrier (BBB) required to maintain normal brain function, are highly sensitive to perturbations under ischemic conditions (37). Thus, administration of a RIPK1 inhibitor after stroke may provide opportunity to reduce BBB damage as well as protect neurologic function by inhibiting both necroptosis and apoptosis.

Methods

Animals. Lyz2Cre/Cre mice and EmxCre/Cre mice were purchased from The Jackson Laboratory (stock nos. 004781 and 005628). All animals were maintained in a pathogen-free environment, and experiments were conducted according to the protocols approved by Harvard Medical School's Institutional Animal Care and Use Committee. The $Ripk3^{-/-}$ mice were a gift from Vishva Dixit, Genentech. The $MAP3K7^{fl/fl}$ mice were a gift from Dr. Shizuo Akira, Osaka University.

Mouse Genotyping. Tak1(f/f) genotyping used the following primers (5′>3′): reverse: GGAACCCGTGGATAAGTGCACTTGAAT; forward: GGCTTTCATTGTGGAGGTAAGCTGAGA. Lyz2Cre genotyping used the following primers (5′>3′): common: CTTGGGCTGCCAGAATTTCTC; WT forward: TTACAGTCGGCCAGGCTGAC; mutant forward: CCCAGAAATGCCAGATTACG. EmxCre genotyping used the following primers (5′>3′): WT forward: AAG GTG TGG TTC CAG AAT CG; mutant forward: GCG GTC TGG CAG TAA AAA CTA TC; WT reverse: CTC TCC ACC AGA AGG CTG AG; mutant reverse: GTG AAA CAG CAT TGC TGT CAC TT. Other mouse genotyping protocols followed the published literature.

Induction of MCAO. Animal experiments were performed following the STAIR guidelines and in accordance with our institutional guidelines and following an animal protocol approved by Harvard Medical School's Institutional Animal Care and Use Committee. All mice were in a C57BL/6 background. C57BL/6 mice (23 to 28 g, 7 to 9 wk) were anesthetized with 3% isoflurane and maintained on 1.2% isoflurane in 70% nitrous oxide and 30% oxygen. rCBF was monitored using a laser Doppler (Perimed) equipped with a flexible probe. Rectal temperature was maintained between 36.5 °C and 37.5 °C with a homeothermic blanket. The right common carotid artery was exposed and clipped. After ligation of the pterygopalatine artery, the internal carotid artery was exposed, and a temporary clip was applied to interrupt blood backflow from the cerebrum. Through a cut external carotid artery, a silicon coated nylon monofilament (Doccol; 602134 PK10) was placed into the internal carotid artery to confirm rCBF dropping to 80% of its former value. All data except that in Fig. 4*J* were from mice with a >80% reduction of blood flow. Less than 10% of the mice with MCAO had a <80% reduction of blood flow and were excluded. In Fig. 4*J*, we used six mice with <80% rCBF reduction for testing whether a moderate reduction of blood flow in the brain could reduce TAK1. After a 60-min occlusion, the filament and the clip were withdrawn, and the mice were kept at 37 °C for 30 min. In a permanent occlusion stroke model, mice were maintained with the filament in and had the same duration of anesthesia and postoperative heat insulation. For sham surgery, all of the arteries were exposed for the surgical period, but the filament was not inserted deeply enough to produce a rCBF change. The surgical period and the anesthesia volume were the same as in MCAO surgery.

Mice were monitored three times a day for the first 24 h, then twice a day for the first week. Buprenorphine 0.08 mg/kg s.c. was given during the recovery period to animals exhibiting signs of pain. Using chiasma as a landmark, the brains from 1 mm anterior to 2 mm posterior to the stroke lesion were used for

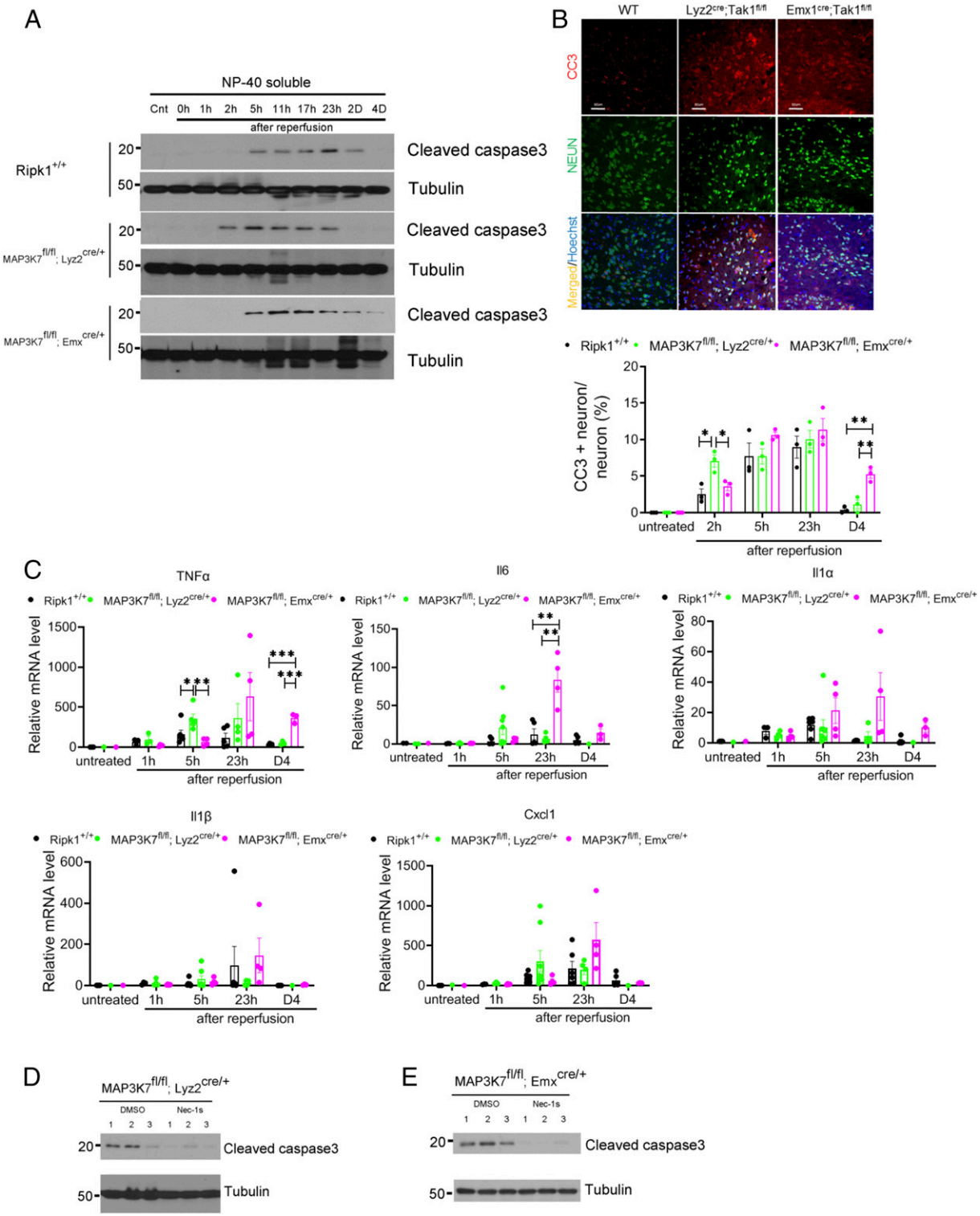

Fig. 6. Selective loss of TAK1 from microglia/infiltrated macrophages or neurons promotes apoptosis. (*A*) The brain lysates from mice with indicated genotypes reperfused for indicated periods after 60 min of MCAO were analyzed by immunoblotting for CC3 and Tubulin. (*B*, *Upper*) Brain sections of WT, *MAP3K7*$^{fl/fl}$; *Lyz2*$^{cre/+}$, and *MAP3K7*$^{fl/fl}$; *Emx*$^{cre/+}$ mice treated with MCAO for 60 min followed by reperfusion for 23 h were immunostained for CC3. (*B*, *Lower*) Quantifications of CC3^{+} neurons is shown at the bottom. $n = 3$ mice for each time point. The data represent mean ± SEM. Assessment of each time point includes data from five sections for approximately 150 cells in each mouse. (Magnification: 40×; Scale bar: 50 μm.) (*C*) Quantitative RT-PCR analysis of the mRNA expression of indicated cytokines and chemokines in the brains of WT, *MAP3K7*$^{fl/fl}$; *Lyz2*$^{cre/+}$, and *MAP3K7*$^{fl/fl}$; *Emx*$^{cre/+}$ mice subjected to 60 min of MCAO followed by reperfusion at different time periods. $n = 4$ mice per time point. The data represent mean ± SEM. (*D*) *MAP3K7*$^{fl/fl}$; *Lyz2*$^{cre/+}$ mice were subjected to 60 min of MCAO and then given vehicle only or Nec-1s(20 mg/kg) i.p. at 0 h and 17 h after the onset of MCAO. The brain lysates from *MAP3K7*$^{fl/fl}$; *Lyz2*$^{cre/+}$ mice reperfused for 23 h after 60 min occlusion were analyzed by immunoblotting for CC3 and Tubulin. (*E*) *MAP3K7*$^{fl/fl}$; *Emx*$^{cre/+}$ mice were subjected to 60 min of MCAO and then given vehicle only or Nec-1s(20 mg/kg) i.p. at 0 h and 17 h after the onset of MCAO. The brain lysates from *MAP3K7*$^{fl/fl}$; *Emx*$^{cre/+}$ mice reperfused for 23 h after 60 min of occlusion were analyzed by immunoblotting for CC3 and Tubulin. *$P < 0.05$, **$P < 0.01$, and ***$P < 0.001$.

isolating protein and RNA. Each experiment was repeated more than three times. Male mice (age 7 to 10 wk) were used in this study. A total of 112 WT male mice, 77 *Ripk1*$^{D138N/D138N}$ mice, 81 *Ripk3*$^{-/-}$ male mice, 53 *MAP3K7*$^{fl/fl}$; *Lyz2*$^{cre/+}$ male mice, and 57 *MAP3K7*$^{fl/fl}$; *Emx*$^{cre/+}$ male mice were subjected to the MCAO procedure. The mortality rate was 4.4% (5 of 112) in WT mice, 2.6% (2 of 77) in *Ripk1*$^{D138N/D138N}$ mice, 3.7% (3 of 81) in *Ripk3*$^{-/-}$ mice, 7.5% (4 of 53) in *MAP3K7*$^{fl/fl}$; *Lyz2*$^{cre/+}$mice, and 5.2% (3 of 57) in *Emx*$^{cre/+}$ mice. There was no significant difference in mortality among these groups. No animals died from the sham procedure.

Measurement of Infarct Volume and Hemorrhage. Mice were sacrificed with an overdose of isoflurane and transcardially perfused with PBS to remove intravascular blood. Coronal brain sections (1 mm thick) were incubated 1% triphenyltetrazolium chloride (TTC) solution (Sigma-Aldrich) at room temperature for 20 min. Infarct volumes were quantified with ImageJ software. We used the indirect method to eliminate confounding effects of edema. Infarct volumes from each slice were integrated to yield the total ischemic lesion volume (38). With the same images, we defined scarlet dot lesions within the area of ischemia as hemorrhagic infarction (37).

Measuring Hemorrhagic Blood Volume. Hemorrhagic blood volume was quantified spectrophotometrically using the QuantiChrom Hemoglobin Assay Kit (BioAssay Systems), in accordance with the manufacturer's recommendations. The hemoglobin concentration was expressed as micrograms per sample.

Quantification of Immunostaining. Tissue sections were immunostained with different Abs, as indicated in the figure legends. The quantification was conducted on five sections from each mouse for ~100 to 150 cells.

Antibodies. TAK1 (Cell Signaling Technology, catalog no. 5206; Santa Cruz Biotechnology, catalog no. sc166562), RIPK1 (BD Biosciences, catalog no. 610459; Cell Signaling Technology, catalog no. 3493), p-RIPK1(S166) (Cell Signaling Technology, catalog no. 31122; MJS BioLynx), CC3 (Cell Signaling Technology, catalog no. 9664), TNFR1 (Cell Signaling Technology, catalog no. 13377), IBA-1 (Wako, catalog no. 019–19741), NEUN (Millipore Sigma, MAB377X), RIPK3 (Abcam, catalog no. ab72106), MLKL (Abcam, catalog no. ab172868), p-RIPK3(T231/S232) (Cell Signaling Technology, catalog no. 57220), p-MLKL (Cell Signaling Technology, catalog no. 37333), LC3B (Cell Signaling Technology, catalog no. 2775), p-p38 (Cell Signaling Technology, catalog no. 9211),p38 (Cell Signaling Technology, catalog no. 9212), p-ERK (Cell Signaling Technology, catalog no. 4370), and ERK (Cell Signaling, catalog no. 9102)

Primary Microglia Culture. In brief, forebrains of 1- to 2-d-old mouse pups were digested with 0.01% trypsin and triturated with DMEM containing 10% heat-inactivated FBS and 1% penicillin-streptomycin. Dissociated cells were plated onto poly-D-lysine–coated 75-cm^2 flasks and fed every 3 d for 7 to 10 d. Following an initial 1-h shake of the culture, microglia were collected and cultured in DMEM + 10% FBS.

Primary Neuron Culture. In brief, forebrains of E15 embryos were digested with 0.01% trypsin and triturated with DMEM containing 10% heat-inactivated FBS and 1% penicillin-streptomycin. Dissociated cells were plated onto poly-D-lysine–coated 24-well plate at density of 2×10^5 cells/well with DMEM. On the next day, the medium was switched to neurobasal medium with 2% B27 supplement (Thermo Fisher Scientific, catalog no. 17504044), and 5 μM cytokine arabinoside was added on day 4. The neurons were harvested on day 11.

Histology and Immunochemistry. Animals were sacrificed and perfused with PBS followed by 4% paraformaldehyde, and 25-μm brain cross-sections were prepared on a cryostat. For immunostaining, tissue sections were mounted and blocked with 10% normal goat serum and 1% BSA, and then incubated with primary antibodies at 4 °C overnight. Images were collected with a Nikon Ti-E confocal microscope equipped with an A1R scan head with spectral detector and resonant scanners; images were acquired with Nikon NIS-Elements software. For each image point, *z* series optical sections were collected with a step size of 0.2 μ, using a Prior Scientific ProScan focus motor. Gamma, brightness, and contrast were adjusted on displayed images (identical for compared image sets) using Fiji software.

Statistics and Bioinformatics. Differences were considered statistically significant at $P < 0.05$(*), $P < 0.01$ (**), or $P < 0.001$(***). Data are expressed as mean ± SEM. Sample sizes for animal studies were determined by power calculations based on pilot studies. JMP version 14.0.0 was used for statistical analyses. Pairwise comparisons between two groups were performed using the Student *t* test. For multiple comparisons among the three genotypes, we performed one-way ANOVA to analyze the difference in means for continuous variables with a normal distribution. Two-way ANOVA was performed to analyze the differences in mean with multiple comparisons over time. When one- or two-way ANOVA showed significant differences, pairwise comparisons between means were tested by appropriate post hoc tests. Behavior assessment was done in a double-blinded manner with a scorer unaware of the previous treatment or genotypes.

Data Availability. All data are included in the manuscript and *SI Appendix*.

ACKNOWLEDGMENTS. We thank Dr. Vishva Dixit of Genentech for the *Ripk3*$^{-/-}$ mice and Dr. Shizuo Akira of Osaka University for *MAP3K7*$^{fl/fl}$ mice. This work was supported by National Institute on Aging Grants RF1AG055521 and R21AG059073. M.G.N. was supported in part by the Fellowship of Astellas Foundation for Research on Metabolic Disorders.

1. M. A. Moskowitz, E. H. Lo, C. Iadecola, The science of stroke: Mechanisms in search of treatments. *Neuron* **67**, 181–198 (2010).
2. A. Degterev *et al*., Chemical inhibitor of nonapoptotic cell death with therapeutic potential for ischemic brain injury. *Nat. Chem. Biol.* **1**, 112–119 (2005).
3. J. Yuan, B. A. Yankner, Apoptosis in the nervous system. *Nature* **407**, 802–809 (2000).
4. A. Degterev *et al*., Identification of RIP1 kinase as a specific cellular target of necrostatins. *Nat. Chem. Biol.* **4**, 313–321 (2008).
5. A. Degterev, D. Ofengeim, J. Yuan, Targeting RIPK1 for the treatment of human diseases. *Proc. Natl. Acad. Sci. U.S.A.* **116**, 9714–9722 (2019).
6. B. Shan, H. Pan, A. Najafov, J. Yuan, Necroptosis in development and diseases. *Genes Dev.* **32**, 327–340 (2018).
7. D. Wallach, T. B. Kang, C. P. Dillon, D. R. Green, Programmed necrosis in inflammation: Toward identification of the effector molecules. *Science* **352**, aaf2154 (2016).
8. P. Amin *et al*., Regulation of a distinct activated RIPK1 intermediate bridging complex I and complex II in TNFα-mediated apoptosis. *Proc. Natl. Acad. Sci. U.S.A.* **115**, E5944–E5953 (2018).
9. Y. Dondelinger *et al*., RIPK3 contributes to TNFR1-mediated RIPK1 kinase-dependent apoptosis in conditions of cIAP1/2 depletion or TAK1 kinase inhibition. *Cell Death Differ.* **20**, 1381–1392 (2013).
10. Z. J. Chen, Ubiquitination in signaling to and activation of IKK. *Immunol. Rev.* **246**, 95–106 (2012).
11. J. Geng *et al*., Regulation of RIPK1 activation by TAK1-mediated phosphorylation dictates apoptosis and necroptosis. *Nat. Commun.* **8**, 359 (2017).
12. Xu D *et al*., TBK1 suppresses RIPK1-driven apoptosis and inflammation during development and in aging. *Cell* **174**, 1477–1491 e19 (2018).
13. A. S. Go *et al*.; American Heart Association Statistics Committee and Stroke Statistics Subcommittee, Executive summary: Heart disease and stroke statistics—2013 update. A report from the American Heart Association. *Circulation* **127**, 143–152 (2013).
14. D. Ofengeim *et al*., Activation of necroptosis in multiple sclerosis. *Cell Rep.* **10**, 1836–1849 (2015).
15. Y. S. Cho *et al*., Phosphorylation-driven assembly of the RIP1-RIP3 complex regulates programmed necrosis and virus-induced inflammation. *Cell* **137**, 1112–1123 (2009).
16. S. He *et al*., Receptor interacting protein kinase-3 determines cellular necrotic response to TNF-alpha. *Cell* **137**, 1100–1111 (2009).
17. L. Sun *et al*., Mixed lineage kinase domain-like protein mediates necrosis signaling downstream of RIP3 kinase. *Cell* **148**, 213–227 (2012).
18. Y. Ito *et al*., RIPK1 mediates axonal degeneration by promoting inflammation and necroptosis in ALS. *Science* **353**, 603–608 (2016).
19. K. Shi *et al*., Global brain inflammation in stroke. *Lancet Neurol.* **18**, 1058–1066 (2019).
20. J. Yuan, P. Amin, D. Ofengeim, Necroptosis and RIPK1-mediated neuroinflammation in CNS diseases. *Nat. Rev. Neurosci.* **20**, 19–33 (2019).
21. A. Das *et al*., Impairment of an endothelial NAD^+-H_2S signaling network is a reversible cause of vascular aging. *Cell* **176**, 944–945 (2019).
22. K. Srinivasan *et al*., Untangling the brain's neuroinflammatory and neurodegenerative transcriptional responses. *Nat. Commun.* **7**, 11295 (2016).
23. Y. Zhang *et al*., An RNA-sequencing transcriptome and splicing database of glia, neurons, and vascular cells of the cerebral cortex. *J. Neurosci.* **34**, 11929–11947 (2014).
24. Y. Chen *et al*., Necrostatin-1 improves long-term functional recovery through protecting oligodendrocyte precursor cells after transient focal cerebral ischemia in mice. *Neuroscience* **371**, 229–241 (2018).
25. G. Dvoriantchikova, A. Degterev, D. Ivanov, Retinal ganglion cell (RGC) programmed necrosis contributes to ischemia-reperfusion-induced retinal damage. *Exp. Eye Res.* **123**, 1–7 (2014).
26. C. R. Kim, J. H. Kim, H. L. Park, C. K. Park, Ischemia reperfusion injury triggers TNFα-induced necroptosis in rat retina. *Curr. Eye Res.* **42**, 771–779 (2017).
27. W. Li *et al*., Neuroprotective effects of DTIO, a novel analog of nec-1, in acute and chronic stages after ischemic stroke. *Neuroscience* **390**, 12–29 (2018).

28. K. Newton *et al*., RIPK3 deficiency or catalytically inactive RIPK1 provides greater benefit than MLKL deficiency in mouse models of inflammation and tissue injury. *Cell Death Differ.* **23**, 1565–1576 (2016).
29. C. C. Smith *et al*., Necrostatin: A potentially novel cardioprotective agent? *Cardiovasc. Drugs Ther.* **21**, 227–233 (2007).
30. R. Yang *et al*., Necrostatin-1 protects hippocampal neurons against ischemia/reperfusion injury via the RIP3/DAXX signaling pathway in rats. *Neurosci. Lett.* **651**, 207–215 (2017).
31. S. Zhang *et al*., Necrostatin-1 attenuates inflammatory response and improves cognitive function in chronic ischemic stroke mice. *Medicines (Basel)* **3**, E16 (2016).
32. P. Lipton, Lysosomal membrane permeabilization as a key player in brain ischemic cell death: A "lysosomocentric" hypothesis for ischemic brain damage. *Transl. Stroke Res.* **4**, 672–684 (2013).
33. A. P. Qin, H. L. Zhang, Z. H. Qin, Mechanisms of lysosomal proteases participating in cerebral ischemia-induced neuronal death. *Neurosci. Bull.* **24**, 117–123 (2008).
34. Y. D. Wen *et al*., Neuronal injury in rat model of permanent focal cerebral ischemia is associated with activation of autophagic and lysosomal pathways. *Autophagy* **4**, 762–769 (2008).
35. K. Hochrainer, Protein modifications with ubiquitin as response to cerebral ischemia-reperfusion injury. *Transl. Stroke Res.* **9**, 157–173 (2018).
36. T. R. Doeppner *et al*., Systemic proteasome inhibition induces sustained post-stroke neurological recovery and neuroprotection via mechanisms involving reversal of peripheral immunosuppression and preservation of blood-brain barrier integrity. *Mol. Neurobiol.* **53**, 6332–6341 (2016).
37. W. Abdullahi, D. Tripathi, P. T. Ronaldson, Blood-brain barrier dysfunction in ischemic stroke: Targeting tight junctions and transporters for vascular protection. *Am. J. Physiol. Cell Physiol.* **315**, C343–C356 (2018).
38. M. Asahi *et al*., Protective effects of statins involving both eNOS and tPA in focal cerebral ischemia. *J. Cereb. Blood Flow Metab.* **25**, 722–729 (2005).